Pergamon

Int. J. Heat Mass Transfer. Vol. 37, No. 4, pp. 559–570, 1994

0017-9310/94 $6.00+0.00

Drop size measurement in a two-phase swirling flow using image processing techniques

RANGANATHAN KUMAR† and SRIDHARAN KANNAN
Department of Mechanical Engineering, Clemson University, Clemson, SC 29634, U.S.A.

(*Received* 8 *June* 1992 *and in final form* 6 *September* 1993)

Abstract—An experimental study of two-liquid swirling flows in a cylindrical hydrocyclone was conducted using flow visualization and digital image processing. The flow pattern was recorded using a video camera and the resulting flow images at cross-sectional planes were digitized in a personal computer. A technique was developed to measure drop sizes and areas using image enhancement and segmentation techniques. The image was cleaned of noise using a set of image processing algorithms. These algorithms included background noise subtraction, contrast enhancement, median and smoothing filters and gray level thresholding, and had to be applied in that order for accurate drop size measurement. The errors and the uncertainties associated with the technique have been addressed. For the range of oil and water flow rates studied, it was seen that the concentration of oil in any plane of cross section of the cyclone reaches a constant value. For the low flow rates studied, the cyclone behaved more as a mixer than a separator due to a weaker radial pressure gradient. Hence, a simple first order model was used to predict time constants for the two water flow rates used. The possibility of introducing this time constant as a suitable time scale was investigated. An attempt was also made to normalize the data using oil–water flow rate as a parameter. There was not sufficient evidence to show that such a ratio could be a flow parameter in this problem.

INTRODUCTION

CONTAMINATION of the working fluid by a different fluid is a frequent occurrence in various industries. Examples include ships' oily waters discharged into the sea, hydrocarbon contamination of sea during offshore drilling, water droplets in petroleum lines and edible oil contamination. It is also a common problem aboard spacecraft where, in tanks that carry cryogenic fluids, vapor bubbles are formed due to heat leaks. These bubbles, though lighter than the parent liquid, do not settle out, owing to zero gravity. They rather remain randomly distributed in the fluid. These bubbles are known to cause problems in fluid transfer and play a leading role in equipment damage. In all the above examples, the contaminant is of a different density in comparison to the working fluid. Inertial techniques are often desirable to separate the contaminant out. A common method of inertial separation is cycloning. A cyclone operates in a centrifugal pressure field. The two phases in the cyclone being of differing densities, are separated out, the lighter phase moving to the cyclone axis. Industrial cyclones normally serve the purpose of separating solid particles from gases.

Generally a cyclone can be a cylindrical tube, a hollow truncated cone or a combination of both. Numerous papers have been written in the area of cycloning. A different type of cyclone is a cylindrical body in which the working fluid is injected tangentially at one end and removed tangentially at the other (Fig. 1(a)). A cylindrical cyclone has been studied experimentally by Listewnik [1], Baranov *et al.* [2] and Colman and Thew [3]. In order to employ such a cyclone as an effective tool of separation, the flow pattern inside the cyclone has to be understood in detail. The aim of the present study is to investigate the drop size distribution in the two-liquid swirling flow inside a cylindrical hydrocyclone for low flow rates.

Some of the earliest and pioneering works on the industrial cyclones have been published by Rietema and Verver [4] and Kelsall [5]. Van Rossum [6] attempted to separate liquid–liquid emulsions in a conventional cyclone. The dispersed phase in his case was the heavier liquid (water). He reported promising results; however, at higher velocities, although the centrifugal forces required for good separation would be greater, it also resulted in the splitting up of the droplets, thus reducing the cyclone efficiency.

Johnson *et al.* [7] and Thew [8] measured the ability of small cyclones to separate liquid drops from water for various flow rates and drop sizes. They observed that for sufficiently large turbulence levels, break-up of the dispersed phase occurs and restricts performance. This agrees with the findings of Van Rossum [6]. The main difference between liquid–liquid and solid–liquid dispersion is that in the former, the density ratio is much smaller. This means a very high centrifugal force is needed to achieve efficient separation. But in order to attain this, a high-flow velocity is needed which would lead to high shear forces and turbulence causing emulsification of the mixture. It has long been noticed that when a liquid is injected into a flowing continuous phase, the fluid breaks up into smaller droplets. The break-up is attributed to the turbulence in the stream. This breakup has been studied in detail by many authors.

Size distribution measurements and flow visualization were done in liquid–liquid systems by Kubie and Gardner [9] and Govier *et al.* [10]. They found

† Current address: Knolls Atomic Power Laboratory, P.O. Box 1072, Schenactady, NY 12301, U.S.A.

NOMENCLATURE

A	normalized area occupied by oil drops (equation (2))	Q, q	volume flow rate
C	volumetric concentration	t	time
I	intensity	$V_{oil,C.V.}$	volume of oil inside the control volume
I_h	arbitrary, high intensity value	t	time constant
I_{in}	input intensity value	s	interfacial tension.
I_{low}	lower intensity limit for contrast enhancement		
I_{out}	output intensity value	Subscripts	
I_t	threshold gray level	C.V.	control volume
M_{oil}	mass of oil	oil	oil stream
$\dot{m}$	mass flow rate	in	entering stream
P	perimeter of the drop	out	exiting stream.

that the oil–water mixtures exhibited a behavior similar to that of air–water mixtures studied by them previously. The phenomena such as droplet break-up and concentration measurement can be studied by new, unobtrusive techniques such as flow visualization. Flow visualization aided by computerized analysis of associated data has long been employed for various applications such as particle velocimetry (PTV). The interior details of the flow is visualized by illuminating the flow with a sheet of light and imaging scattered radiation from the particles. An extensive and exhaustive overview of this technique was given by Hesselink [11]. Digital image processing in combination with flow visualization is relatively recent. Flow imaging is difficult as compared to natural scenes and medical imaging because the former tends to show fuzzy boundaries between different regions caused by diffusion. This compounds the problem of edge detection.

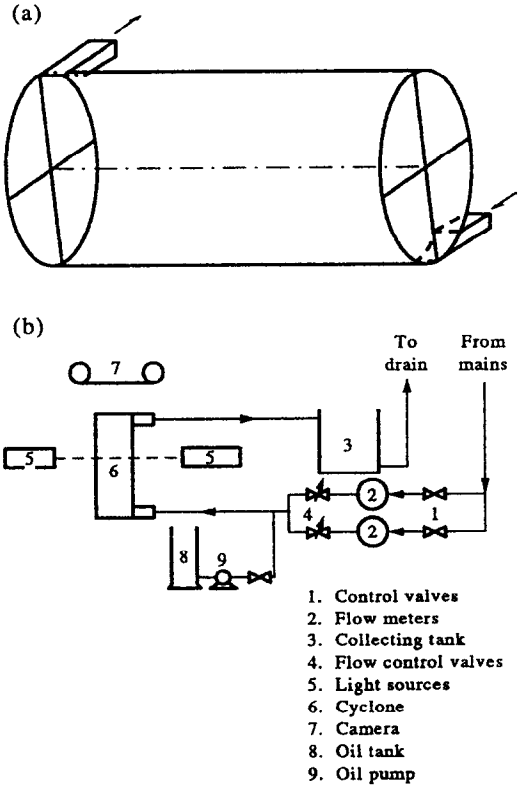

FIG. 1. (a) Experimental cyclone. (b) Experimental arrangement.

Though there is significant literature on the application of image processing in PTV, the literature on its use in the analysis of two liquid flow is scarce. Ow and Crane [12, 13] were among the earliest to employ this technique. They developed an automatic image analysis system and used it for obtaining size distributions of droplets in two-phase flows from multiple photographs with sub microsecond exposure. The software that they had developed contained procedures for detecting and filling in voids in a droplet, rejecting out of focus droplets, etc. The system had the resolution capable of detecting droplets in the range 20–200 microns. More recently, Bertollini *et al.* [14] developed an image processing system that automatically analyzed the size distributions in spray video images. They generated images by using pulsed laser light to freeze the droplet motion under study. These images contained diffraction patterns representing the droplet's degree of focus. Thousands of images were recorded per sample volume to get an ensemble average of the distribution at that volume.

Hanzevack *et al.* [15] studied in detail the two liquid flow phenomenon laser image processing. Their main objective was to determine the various parameters that affect water dispersion in crude oil. Drop size distribution and concentration profiles were determined. A microcomputer based digital image processing system was developed to count and size laser generated images by Ahlers and Alexander [16]. Basic problems and limitations with using a digital image processing system were addressed. The system was calibrated using a standard calibration reticle. A

pattern recognition scheme was developed that was able to count and size the images; the algorithm was similar to that developed by Ow and Crane [12]. The work of Kim and Lee [17] is among the latest endeavors to measure drop sizes using image processing. An efficient system for measuring the size of spherical spray drops was developed and tested. The intensity histogram from the droplet image was simple enough to visually identify the threshold level where drop sizes were accurately measured.

From the literature survey conducted, it can be concluded that no investigation has ever been carried out on the instantaneous behavior of two liquids inside the hydrocyclone, with respect to the concentration and drop size measurement. Different data acquisition techniques have been used in this kind of flow analysis. Due to its unobtrusive nature, ease of operation and enormous future potential, digital image processing is gaining importance in particle sizing. Its reliability has been tested and proven. For these reasons, digital image processing has been adopted as the data acquisition technique in the current study.

The purpose of this research is to study the swirling flow of an oil–water mixture inside a cylindrical hydrocyclone using flow visualization and digital image processing. The specific objectives of this work are to (a) develop a reliable technique for the measurement of instantaneous oil drop size and oil concentration profile on a plane cross section inside the cyclone using digital image processing, and (b) conduct experiments with oil–water mixtures and record the flow field using a video camera and do a parametric study of the oil–water flow in a cyclone for low water and oil flow rates.

EXPERIMENTAL SET-UP AND PROCEDURE

The experimental cyclone is a cylindrical tube with a tangential inlet and a tangential outlet. A diameter of 8 inches was chosen to obtain a good spatial resolution in the photographic scale (at least 2 to 3 pixels occupying 1 mm), and an axial length of 16 inches to maintain an aspect ratio of 2 for initial investigations. The cyclone was made of plexiglas for easy machinability and easy optical access to the flow. The cylinder is sealed on either end by a 1/2 inch plexiglas plate. The cyclone is illustrated in Fig. 1(a). The entry and the exit ports are rectangular with dimensions of 1 inch width and 0.5 inch height. The dimensions of these ports were chosen based on conventional designs. Since the emphasis of this work is to study the flow pattern in swirling flow, the cylinder was mounted horizontally for convenience of flow visualization.

The open loop configuration is illustrated in Fig. 1(b). It consists of two flow meters in parallel, the hydrocyclone, a settling tank, an oil reservoir and an oil pump. Using an oil–water mixture and recirculating it through the pump caused the oil to emulsify with water and hampered flow visualization. For this reason, the open loop technique was used throughout the study. The two flow meters were of rotameter type, having ranges of 6 and 23 GPM, respectively. Provision of two flow meters ensured accurate measurement both at high and low flow rates, although measurements were made in this study for low flow rates. The connections were made by means of 1 inch transparent and flexible vinyl tube. Most of the system was transparent to provide complete optical access. The oil was stored in a 2000 cm^3 capacity, graduated tank. Oil injection was accomplished using a Cole-Parmer 1000 $cm^3\ min^{-1}$ gear pump. Oil flow was controlled using a by-pass mechanism; on-line calibration gave the oil flow rate precisely.

The system used water straight from the supply mains. The oil used was Dow Corning 20cS silicone oil. The oil was injected into the water upstream to the entry port of the cyclone through a 1/8 inch brass tube at about 20 inches upstream of the entry port. This ensured adequate dispersion of oil in water as the mixture entered the cyclone. The oil–water mixture that exits the cyclone was collected in a settling tank.

Flow visualization

The flow visualization was done by illuminating cross sectional planes of the flow perpendicular to the cylinder axis. Two slide projectors were used as light sources simultaneously from either side of the cyclone. The photographic slides were replaced by slits formed by placing two razor blades in close proximity. The projectors were focussed to produce a thin sheet of light across the cylinder, with the focal plane on the cylinder axis. It was found that a slit of 2 millimeters width produced a sheet across the cylinder that was roughly 15 millimeters thick. Since the maximum size of the drops encountered in this research was found to be only about 4 to 5 millimeters, this thickness of the sheet of light was adequate in covering the entire drop in the lit volume most of the time.

The flow pattern of the oil–water mixture was observed and recorded using a JVC S-VHS Video Camera, positioned orthogonal to the plane of light. Since both spatial and temporal variation of the flow pattern were to be studied, continuous videography was preferred over conventional snap-shot photography. A S-VHS camera was preferred due to its better resolution. Oil was dyed with a luminous dye, and the oil drops reflected light preferentially over water which then formed a dark background. This flow pattern was continuously captured by the video camera. A shutter speed of (1/250) seconds was seen to be adequate in terms of flow visualization and freezing the drop motion.

Data acquisition

The data acquisition procedure consisted of playing back the recorded images on the video cassette player. This procedure is termed as 'off line' imaging. The video cassette player was interfaced with a video moni-

tor through an Image Vision PCPlus frame grabber installed in a Personal Computer. As the video tape was played back and scrolled continuously, the images of the flow field were frozen at discrete time steps (every 20 s in the present case). In order that more accurate information is obtained, ensemble averaging of several frames (8 frames in this case) at the same time step was performed. At a tape speed of 30 frames per second, 8 frames correspond to 0.27 seconds. Ensemble averaging improves accuracy by smoothing out the scatter in the data. The difference between the results of 8 frames and 12 frames was found to be small (for a typical experiment, it was 2.5% which was within the uncertainty limits) and it was decided to ensemble average over 8 frames. The frozen frame on the monitor was digitized by the frame grabber. The frame grabber was driven by the Jandel Video Analysis software JAVA. The image was stored as an array of 640 × 480 'picture elements' or 'pixels'.

Data reduction using image processing

Drop sizes and concentration are the primary variables to be measured, and these variables are measured from the images by object counting algorithms. These algorithms work by detecting the edges of the drops, identifying them as individual objects and measuring their sizes. Various techniques involved in image processing, their importance in the current application and their effects on the oil drop size are discussed next.

RESULTS AND DISCUSSION

The present study consists primarily of developing the appropriate sequence of image processing algorithms and subsequently employing the technique to extract flow data. The results are broadly divided into two categories: (i) image processing and (ii) oil concentration results. The first part discusses the effect of the technique on the determination of the drop size and the measures taken to address and reduce the errors and uncertainties. The data that were measured and processed from the experimental runs are then presented and discussed in the second part.

Image processing results

In general, the most useful tools in image processing are the intensity profile and the gray level histogram. A histogram could be a useful tool if it contains definite spikes which could give us some idea regarding the thresholding level (to be discussed later). This was not the case, however, in the current study and hence the intensity profiles were used predominantly to determine the characteristics of a drop.

The intensity profile across a drop is marked by two distinct regions—the background of the drop and the drop itself. Figure 2(a) illustrates the intensity values plotted on the vertical axis at various points on the cross section of a drop. The background is marked by spike like fluctuations in intensity which constitutes the noise which needs to be eliminated from the image. Because the objective here is to measure the size of the drop, we need to specify a certain gray level, called the threshold, whose contour determines the edge of the drop. The intensity profiles of the same drop from successive rows are drawn side by side in Fig. 2(b). Each coordinate point in this curve represents a pixel. Then, the total number of these coordinate points gives the total number of pixels occupied by the drop, and thus the area of the drop. One way to automatically count the number of pixels is to count the number of pixels above the threshold, I_t. But, from line A–H of Fig. 2(b), the image processing algorithm will consider noise to be a legitimate object, which will grossly over predict the object size and number. If, on the other hand, a higher value of I_t is used (say, 40 in this example), then the area of the drop may be under predicted. Thus, it is clear that before the drops are identified and sized, they should first be 'cleaned' of noise if accurate sizing is to be accomplished.

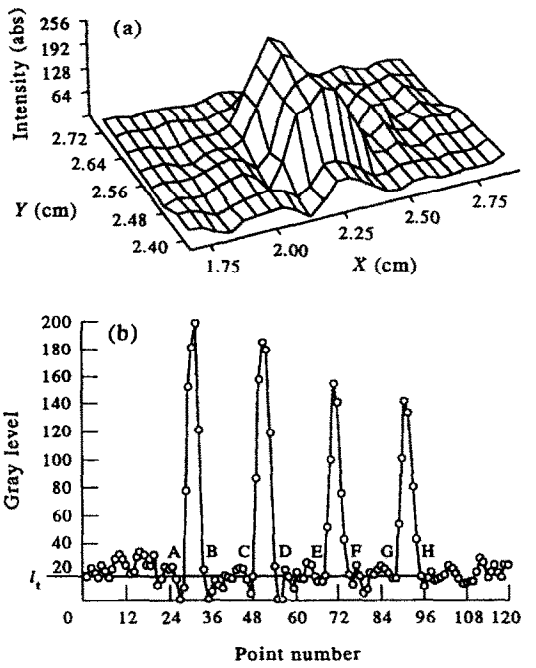

FIG. 2. (a) Three dimensional perspective of intensities of an unprocessed image of a drop. (b) Intensity profiles across the same drop at various cross sections.

Image enhancement techniques

Image enhancement is necessary due to the inherent noise in the image. One type of image noise is random noise, characterized by a statistical variation in the gray level from pixel to pixel. It may originate due to the presence of finely dispersed colloidal particles, or

it may be an inherent part of the image formation process such as granularity in the image. If the noise is uncorrelated from pixel to pixel, its variation can be reduced by the low pass filter.

Another type of noise is called isolated noise. Isolated noise can occur in certain pixels or even in lines due to bit loss in data transmission. Non-linear filtering techniques have been used to remove such specks or streaks.

Background noise subtraction. This is a procedure by which most of the background noise can be subtracted from the original image. In order to suppress the background noise that remains constant in all the images, an image of the flow field is captured prior to introducing the dispersed oil phase. The intensity values of this image are then subtracted from those of the subsequent images with the oil drops. The subtracted image of the flow field of Fig. 3(a) is shown in Fig. 3(b).

Contrast enhancement. Since the gray level histogram had a narrow intensity range, the unprocessed image showed a low contrast. Processing such an image to enhance the contrast would display the information actually available in the digitized image. This is done by linearly stretching a given range of gray levels across a different range of gray levels in the intensity histogram.

The intensity range is defined by the limiting values I_{hi} and I_{low}. For each pixel with intensity at or below I_{low}, the intensity value is reassigned to zero (black). For intensities at or above I_{hi}, the intensity value is reassigned to 255 (white). The remaining pixels undergo a linear transformation mathematically represented as:

$$I_{out} = [(I_{in} - I_{low})/(I_{hi} - I_{low})] \times 255. \quad (1)$$

A suitable value for I_{low} was determined to be between 13 and 18 based on subjective evaluation. While the noise is removed, the drop decreases in size. Contrast enhancement has a profound effect on small drops. The smallest drop reduced in size by as much as 33% although this is not typical of contrast enhancement. The objective of this operation is not only to reveal the intensity variation present in the image, but also to remove or to reduce low intensity noise such as out-of-focus drops. Further, the background noise is not constant from one image to the other, and hence the background subtraction alone does not clean the image entirely.

Spatial filtering. Spatial filtering, like background subtraction and contrast enhancement, is a pixel-by-pixel transformation of the image which depends on the gray levels of the neighboring pixels. It was found in this study that median and smoothing filters had the desired effect.

Median filter is a type of non-linear filter that removes specks and tiny lines which are typical of the noise left behind after the application of contrast enhancement. Median filter replaces the gray level of each pixel with the median value of its 8-pixel neighborhood. The specks are much smaller than the oil drops and are usually contained in 1 or 2 pixels. Since the neighboring pixels are dark with intensity values close to zero, median filter effectively suppresses most of this noise. To make this operation effective, contrast enhancement was applied first so that the background noise could be reduced to tiny specks which were then removed by median filtering. Median filter also smooths out the edges of the drops and in the process, reduces the size of the drops. The processing operations described so far, image subtraction, contrast enhancement and median filter suppressed different types and levels of noise, but at the same time reduced the actual size of the drop.

The smoothing filter operation offsets such effects. This filter replaces the gray level of each pixel in the image with the arithmetic mean of the eight pixel neighborhood. Although this operation has a blurring effect on the image, it is an important part of the sequence of operations in determining the diameter of the drops accurately. In addition, the increase in size during this operation compensates for the reduction in size in all the previous operations. These operations in the given sequence made the intensity profile in Fig. 2(a) appear more symmetric.

Image segmentation. Having enhanced the images to significantly improve their visual quality, a segmentation technique called thresholding was done to clearly identify the objects and size them. Thresholding is a type of contrast manipulation; however, it is not designed to enhance contrast in the sense discussed earlier. Instead, it segments the image into two classes defined by a single gray level threshold. The algorithm used for thresholding is given as follows:

$$\text{if } I_{in} < I_t; \quad \text{then } I_{in} = 0; \quad \text{else}; \quad I_{in} = I_h \quad (2)$$

where I_{in} is the gray level of any pixel, I_t is the threshold intensity, I_h is an arbitrary value. This operation makes the drops look brighter and stand out against the dark background.

Since area measurement is quite sensitive to the threshold level, the correct threshold for the whole image cannot be determined easily. The effect of thresholding on two different drops was shown by Kannan [18]. As the threshold was increased, the diameter decreased, as expected. Determination of threshold by visual inspection led to significant errors. The drops appeared to retain the same size for thresholds of 10 and 20 on the monitor. However, an error of as much as 15% was introduced for the smaller drop when the wrong threshold was selected.

Various methods have been attempted by researchers to remove the subjectivity in determining the threshold level. In the current application, the histograms did not exhibit a clear bimodal distribution and hence this method was not used here. Castleman [19] used the point of maximum slope in the intensity profile as the threshold since this is approximately the point where the human eye places the boundary when viewing an image. This method

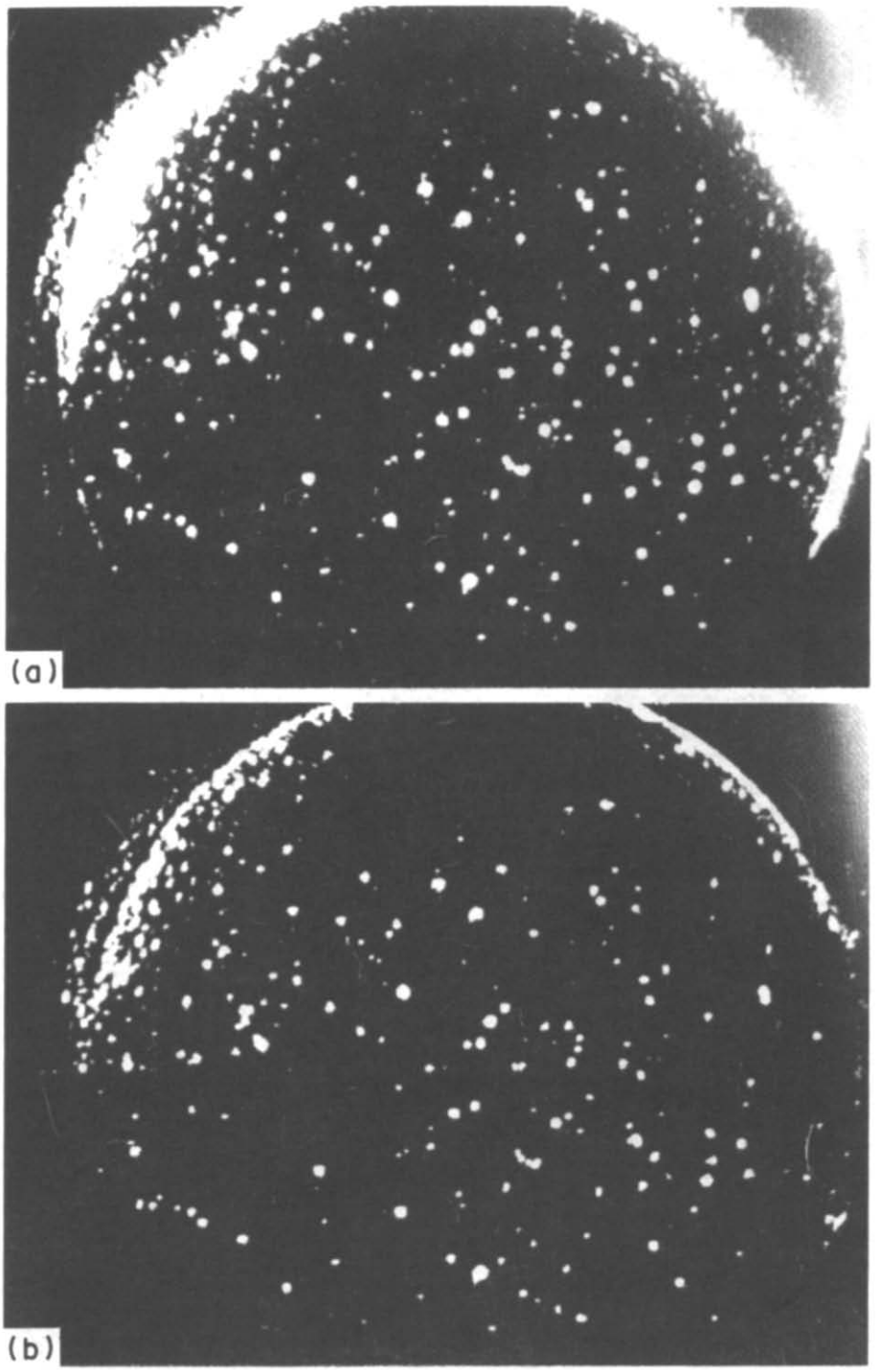

FIG. 3. Effect of image subtraction. (a) Original image. (b) Image after subtraction.

appears to be quite subjective and hence not used. Hanzevack *et al.* [15] employed a technique in which tangents were drawn to the intensity profile used to determine the threshold automatically. Ahlers and Alexander [16] used a calibration reticle to determine the threshold. In their study, the drops occupied at least 100 pixels in area. In the current study, the oil drop occupies as few as 25 pixels. For small drops occupying only a few pixels, no study has been done in the literature to the authors' knowledge and hence there is no known reliable calibration procedure. Magnifying the image to improve resolution is impractical for thousands of image frames. Hence, in the current study, a representative sample of oil drops

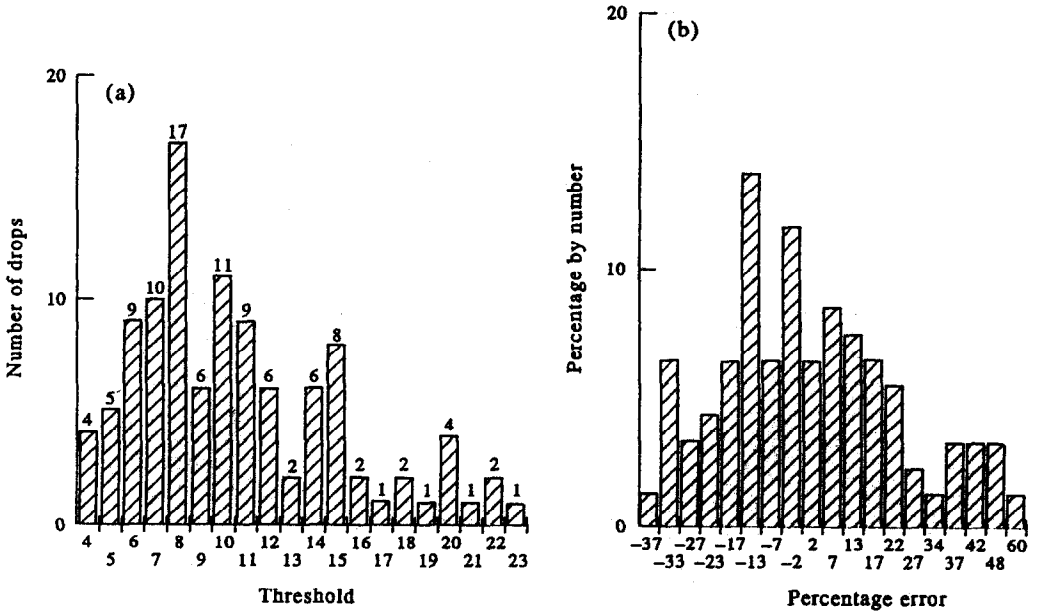

FIG. 4. (a) Distribution of correct threshold. (b) Error for fixed threshold of 10.

from different cross-section frames was identified and sized manually. Such a manual determination of drop size by counting the pixels contributes to uncertainty and its significance will be discussed later.

It is believed in this study that the intensity of the light source was not strong enough to cause a large diffraction pattern around the oil drop. The sharp peak and the sudden drop of the intensity as shown in Fig. 2, to an extent, suggest the same.

Representative drops (more than 100) from different frames were sized by counting the pixels, and thresholded at different levels to verify the correct threshold and to check the effect of wrong threshold levels. The frequency distribution of the correct threshold for these representative drops is given in Fig. 4(a). For all further data analysis of images at different times and frames, a uniform threshold level of 10 was chosen so that thousands of frame data can be acquired in an off-line semi-automatic fashion. For these drops, the error involved in choosing 10 as the threshold was calculated. The error distribution is plotted in Fig. 4(b). The root mean square error is 18.8% and the mean error is 3%. But since the areas of individual drops are simply summed to get the concentration, the simple mean error is an adequate representation of the error involved. A three dimensional perspective of the intensity profile of a processed drop before and after thresholding is given in Fig. 5 and a fully processed image of the flow field after thresholding is shown in Fig. 6.

Shape factor. For each object, a shape factor, $P^2/4A$ was computed, where P is the perimeter and A the area. For a perfect circle, $P^2/4A = \pi$. For any other shape, it is different from π. A practical limiting value of $P^2/4A$, above which objects could be rejected, was determined. Application of filters appeared to have the effect of making the drops look more circular, as

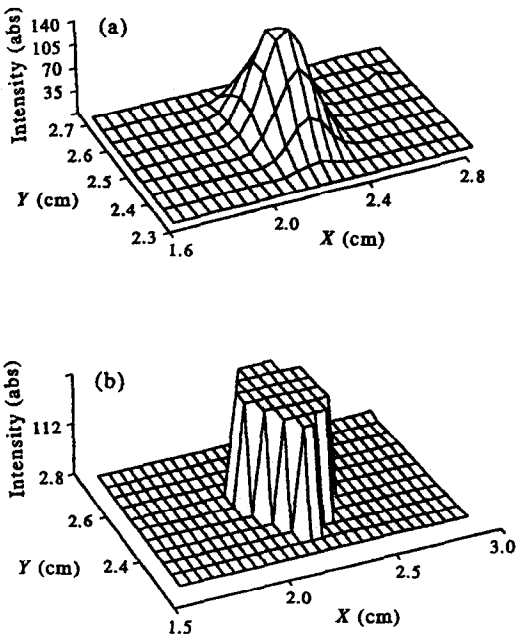

FIG. 5. Three dimensional perspective of intensities for (a) processed image before thresholding, (b) processed image after thresholding.

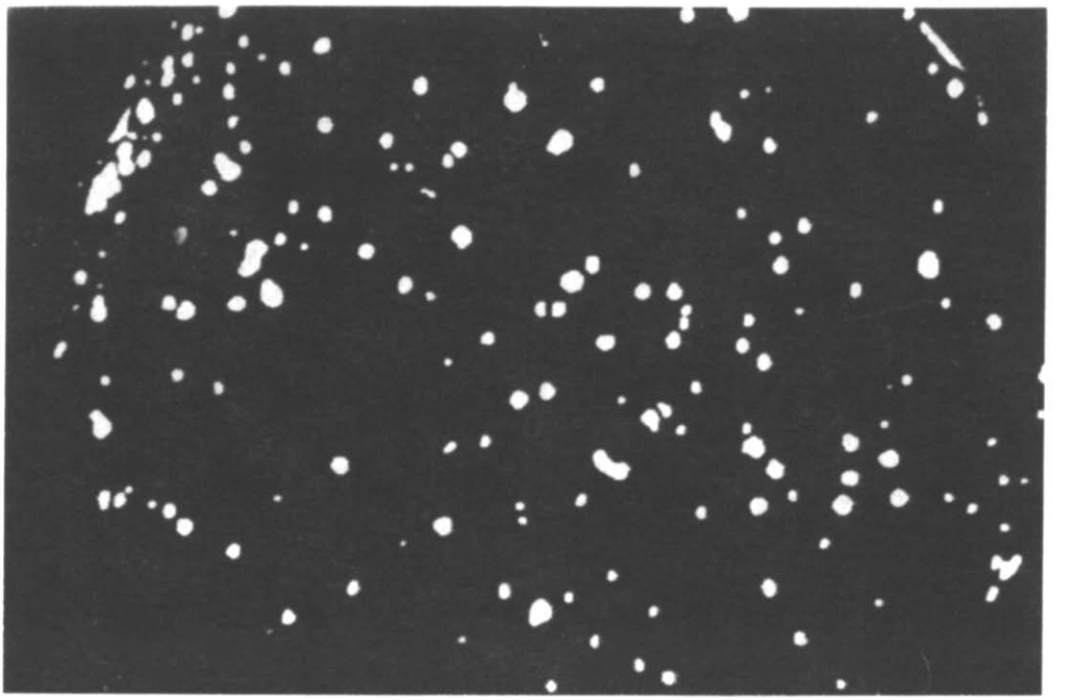

FIG. 6. Flow field after image segmentation.

evident from the values of $P^2/4A$. A practical value of the ratio between $P^2/4A$ and π equal to 1.2 was chosen arbitrarily to automatically eliminate artifactual streaks. When thresholding is involved in digital processing, semi-automation is better than completely automated on-line processing.

Since a new technique has been employed to study a complicated flow pattern, the current study warrants further studies in the technique employed and the data that could be extracted. Following are some of the recommendations for future work.

Digital image processing is an extremely memory intensive operation. It was found that each image of a typical flow field occupies about 250 kilobytes of disk space. A typical experiment is run for 5 min and the data is collected every 20 s, with 8 frames being ensemble averaged at every instant. In short, a typical experimental run would require 120 frames to be analyzed. About twenty separate experiments were conducted in the present study for the purpose of reproducibility as well as ensembling averaging. These runs correspond to 2400 images or 600 megabytes of memory. This is about 5 times the capacity of a regular hard drive of a personal computer. Some of the solutions to the storage problems associated with Digital Image Processing include compressing the image files, using external disk drives such as optical drives, etc. The storage problems of image processing have to be addressed before it can be used for elaborate data reduction.

Errors and uncertainties

There are certain inherent uncertainties associated with using digital image processing as a data reduction tool for oil drop size measurement. The errors associated with the technique can be broadly classified as: (1) errors due to image processing, (2) errors inherent in calibrating the system. By predicting the errors due to threshold selection, the errors due to image processing are automatically addressed. These errors were computed as shown in the previous section.

Error due to pixel resolution is a calibration error, since the error is introduced while calibrating the system by manually counting the number of pixels occupied by the drops. The uncertainty is represented as a percentage of the total number of pixels occupied by the drop, and its distribution was plotted (not shown here) and the average error was 14.7% and the RMS error was 15.4%.

A more generalized and complete uncertainty analysis was done. The errors were grouped as random or precision errors and bias errors. The errors were further classified into (i) calibration errors, (ii) data acquisition errors and (iii) data reduction errors. Table 1 lists the uncertainties. For a typical run, the average uncertainty based on the above analysis was found to be between 25 and 30%.

Concentration results

The image processing technique developed was used in taking some preliminary data with regards to oil concentration in water. The projected areas of all the drops in a given cross section were added to give the oil concentration for that cross section. This was then plotted as a function of time to give the temporal variation of concentration in any given cross section. This variation was studied in different cross sections

Table 1. List of uncertainties

Classification	Number	Description	Type	Value
Calibration	1	Error in the area of the calibration square	Bias	2%
	2	Error in the positioning of the calibration square	Bias	<0.5%
	3	Error due to the pixel resolution of the calibration error	Bias	2%
	4	Pixel resolution error in the manual counting of drops	Bias	15.4% (RMS)
Data acquisition	5	Water flow meter uncertainty	Bias	1%
	6	Oil flow uncertainty	Bias	2.3%
	7	Drops being partly in the illuminated plane	Random	<15%
	8	Drops forming streaks	Random	<1 pixel
Data reduction	9	Due to image processing routines	Random	—
	10	Due to threshold selection	Random	18.8% (RMS)

of the cylinder by varying parameters such as (i) oil flow rate and (ii) water flow rate. Two water flow rates of 4 and 5 GPM, and at least five different oil flow rates ranging from 0.01 to 0.04 GPM were used. Because the oil flow rate was small, it was calibrated for each experiment. In this way, the minor variations in oil flow rate were accounted for, and an average value of the flow rate was noted by directly measuring the volume of the oil dispersed.

Concentration of oil in a given plane was obtained by adding the area of all the oil drops present in a plane. Readers are reminded that the term 'concentration' refers to the area concentration here (not based on volume, as is usually done).

Temporal variation of concentration. In observing the variation of oil concentration with time, a distinct factor was noticed: the oil concentration always increased with time in a given cross section up to an extent, after which it more or less remained the same (Fig. 7(a)). The time it takes to attain this stationary state, however, seems to depend on various factors such as oil flow rate, water flow rate, etc. This indicates that at least for the low flow rates of water to which the present study was confined, the oil does not reside inside the cyclone, but is rather forced out in a steady stream with water. At high water flow rates, however, due to the higher centripetal pressure gradient, oil may be forced towards the center of the cylinder and may reside for longer periods, contributing to statistically non-stationary patterns in concentration.

This behavior of oil, where the concentration increases initially with time and then levels off may be due to the fact that in the absence of a strong radial pressure gradient, the cyclone acts more as a mixer than a separator. To test this, the cyclone was modeled as a first order system, similar to a well stirred reactor, a well researched problem. The development of this model and the resulting analysis are presented in the Appendix. This model predicts an exponential increase in oil concentration in the cylinder, with a time constant given by the ratio of the volume of the cyclone to the total volume flow rate. The approximate time constants for 5 and 4 GPM flow rates were calculated to be 42 and 53 s, respectively. Figure 7 indicates that the oil concentration in any plane levels off within 2–3 time constants, confirming that at low flow rates of water encountered, the cyclone resembles a continuously stirred reactor.

Effect of water and oil flow rates. Water flow rate was seen to have a pronounced effect on oil concentration. In Fig. 7(a), it is clear that in a given cross-sectional plane (in this case, 136 mm), as the ratio of oil to water flow rates increases, concentration of oil increases. For the same oil flow rate (for ratios of 3.87 and 5.43 in the same figure), oil concentration was always higher for the lower water flow rate. In general, the higher the ratio between the oil and water flow rates, the higher is the concentration of oil in the plane, at least for the given low oil or water flow rates.

Based on the deduction that the area occupied by oil in a cross section increases with oil–water flow rate ratio, and that a reactor model may be appropriate for this flow situation, area and time were scaled as follows for a cross-section of the cylinder:

$$A = \frac{\text{(oil drop area/cross-sectional area)}}{\text{(ratio of oil–water flow ratio)}}$$

$$t = \frac{\text{actual time}}{\text{time constant}}.$$

These normalized variables were then plotted on a log–log graph as given in Fig. 7(b). The data seem to follow the relationship,

$$A = C \cdot t^n. \tag{3}$$

The values C and n seem to depend upon a different parameter as yet unknown.

Concentration at different cross sections. With a view to comparing the concentration variation with time at various cross sections, selected experiments were done with the oil and water flow rates held constant, and concentration was plotted against time for each cross section. The results are shown in Figs. 7(c)–(f) for axial locations of 255 mm (near the middle of the cylinder) and 305 mm (near the exit of the cylinder). For flow ratios below 3.5×10^{-3}, oil content in these cross sections is nearly the same; however, as the flow ratio is increased, the oil content increases disproportionately. For example, in Fig. 7(e), as the flow ratio is doubled (maintaining the water flow rate

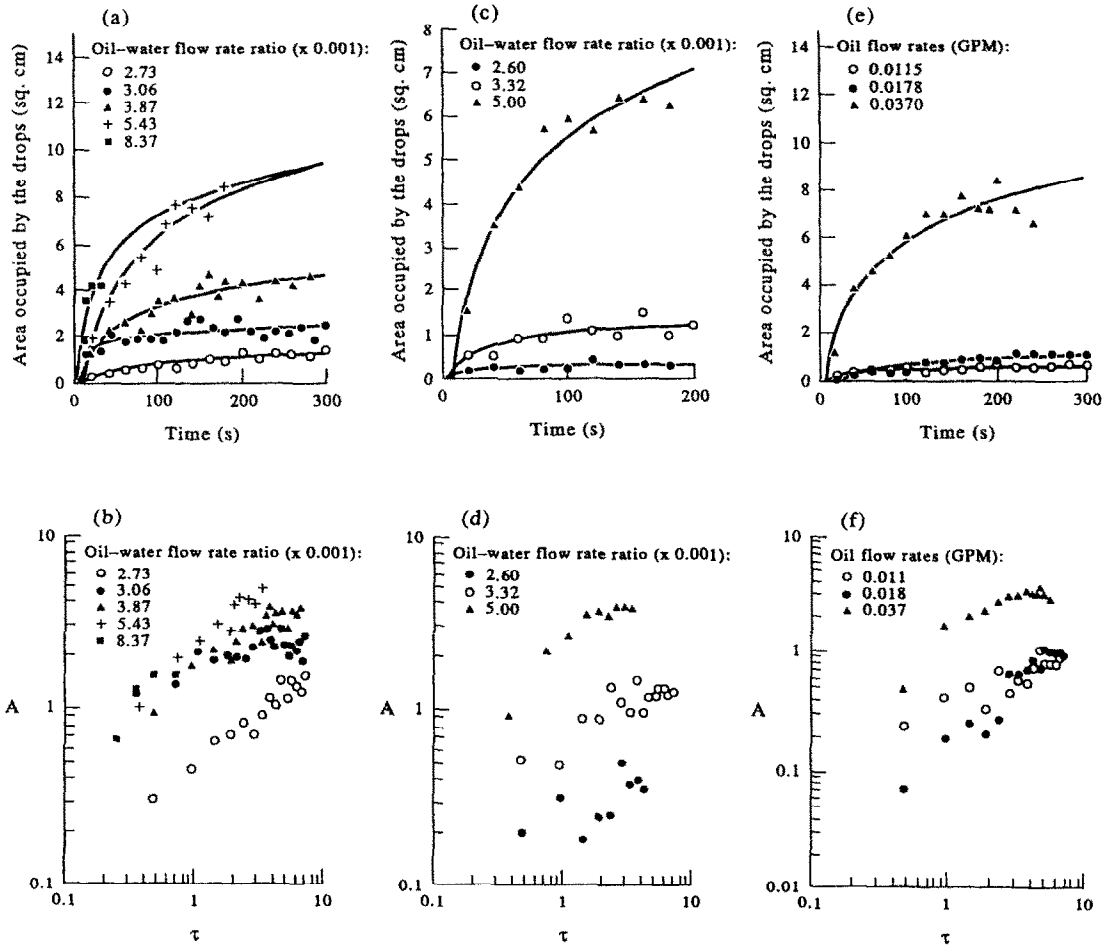

FIG. 7. Effect of oil–water flow rate ratio on area concentration at (a), (b) 136 mm from the inlet; (c), (d) 244 mm from the inlet; (e), (f) 305 mm from the inlet.

constant), the oil content increases nearly eight-fold. The data for each flow rate ratio appear to follow the relationship given in equation (3) although the scatter is wider for lower oil flow rates.

The effect of water flow on concentration for the same oil flow rate at 255 and 305 mm are given in Fig. 8. In these experiments, the oil flow rate was kept constant at 1.85×10^{-2} GPM. Three observations may be made. The first is that at both cross sections, the area occupied by oil is seen to be disproportionately higher for the lower water flow rate of 4 GPM. Secondly, for the same flow rates, the cross section near the exit retains more oil than the one in the middle. Finally, comparing Figs. 8(c) and 7(e), in the same cross section (i.e. 305 mm), there appears to be a discrepancy that the area occupied by the oil drops is considerably lower for the higher flow rate ratio. In this case, however, the higher flow rate ratio was arrived at by using a water flow rate of 5 GPM instead of 4 GPM. These observed trends suggest that either A is not the appropriate parameter or that there is another parameter that plays an important role in this flow situation.

CONCLUSIONS

An image processing technique was employed in the current study to understand two-liquid swirling flows by instantaneous visualization of the flow pattern. While image processing has been employed extensively in velocimetry and to a lesser extent in two phase pipe flows, its application to explain two phase rotating flow is new. The present study consisted of developing the technique and using it to extract phase distribution data. The conclusions are summarized below.

1. The image processing technique has been tested and proven to be a practical and reliable means to measure oil drop size and concentration even for drops that occupied as few as 25 pixels. The uncertainty in our measurements was estimated to be between 25 and 30%.

2. In order for accurate data reduction to be made, certain image processing routines were performed prior to drop identification and subsequent size measurement. These routines had to be applied in a certain order identified in this study to yield accurate

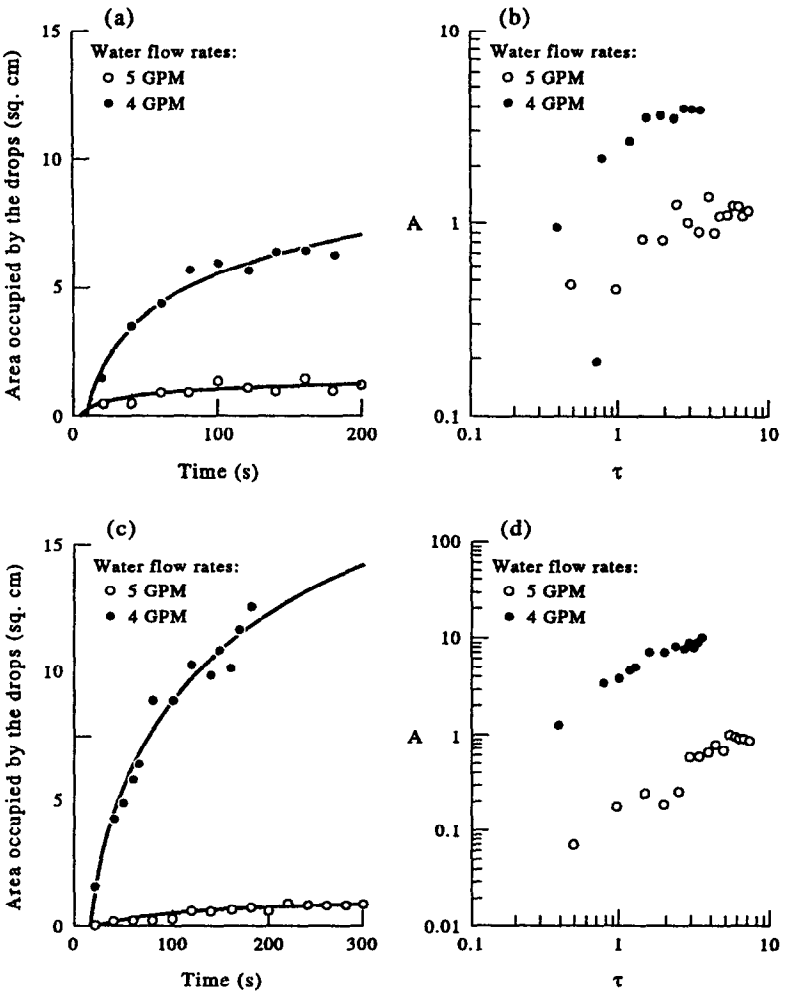

FIG. 8. Effect of water flow on area concentration for an oil flow rate of 1.9×10^{-2} GPM at (a), (b) 255 mm from the inlet; (c), (d) 305 mm from the inlet.

data. The order consists of background subtraction, contrast enhancement, median and smoothing filters and gray level thresholding. Image processing was carried out in two steps, namely, image enhancement and image segmentation. It not only eliminates noise to measure drop size accurately, but also restores the drop to a circular shape.

3. The value of threshold gray level is critical for edge detection and drop size measurement. The size of the drop was seen to vary significantly with threshold. This is because of the shape of the intensity profile across a drop which uniformly increases to a maximum at the center of the drop. Thresholding is seen to be a subjective procedure; a semi-automatic procedure has been developed to apply the correct threshold. A threshold gray level of around 8–12 applied after image processing yielded good results in the current flow situation.

4. The oil concentration in the cyclone increased monotonically with time until it levelled off. This suggested that at the low flow rates of water encountered in this study, the cyclone behaved more as a first order mixer than a separator. This is due to the absence of sufficient centripetal pressure gradient to produce cyclonic flow.

5. The oil concentration in the cylone depended strongly both on the water and the oil flow rates. Results suggest that the ratio of oil to water flow rates would not be the only parameter governing the flow situation.

6. For lower values of oil–water flow rate ratios, the oil concentration did not show any marked change along the length of the cyclone. At higher flow rate ratios, however, there was variation to a large extent, especially when the water flow rate was varied.

Acknowledgements—This work was partially supported by NASA Kennedy Space Center under grant # NAG 10-0056.

REFERENCES

1. J. Listewnik, Some factors influencing the performance of de-oiling hydrocyclones for marine applications. *Proc.*

2nd Int. Conf. on Hydrocyclones, Bath, England, BHRA, 19–24 Sept. (1984).
2. D. A. Baranov, A. M. Kutepov and I. G. Ternovskii, Flow-rate characteristics and hydrodynamics of a counterflow cylindrical hydrocyclone, *J. Appl. Chem. USSR.* **57**(5), 1181–1184 (1984).
3. D. A. Colman and M. T. Thew, Correlation of separation results from light dispersion hydrocyclones. *Chem. Engng Res. Des.* **61**, 233–240 (1983).
4. K. Rietema and P. G. Verver (Editors), *Cyclones in Industry*. Elsevier, Amsterdam (1961).
5. D. F. Kelsall, A study of the motion of solid particles in a hydraulic cyclone, *Trans. Inst. Chem. Engrs* **30**, 87–104 (1952).
6. J. J. Van Rossum, Separation of emulsions in a cyclone. In *Cyclones in Industry* (Edited by K. Rietema and C. G. Verver), pp. 110–117. Elsevier, Amsterdam (1961).
7. R. A. Johnson, W. E. Gibson and D. R. Libby, Performance of liquid–liquid cyclones, *Ind. Engng Chem. Fundam.* **15**(2), 110–115 (1976).
8. M. Thew, Hydrocyclone redesign for liquid–liquid separation, *The Chemical Eng.*, 17–23, Jul/Aug (1986).
9. J. Kubie and G. C. Gardner, Drop sizes and drop dispersion in straight horizontal tubes and helical coils, *Chem. Engng Sci.* **32**, 195–202 (1977).
10. G. W. Govier, G. A. Sullivan and R. K. Wood, The upward vertical flow of oil–water mixtures, *Can. J. Chem. Engng* 67–75 (April 1961).
11. L. Hesselink, Digital image processing in flow visualization, *Ann. Rev. Fluid Mech.* **20**, 421–485 (1988).
12. C. S. Ow and R. I. Crane, A simple off-line image processing system with application to drop sizing in two-phase flows, *Int. J. Heat Fluid Flow* **2**(1), 47–53 (1980).
13. C. S. Ow and R. I. Crane, Pattern recognition procedures for a television–minicomputer spray droplet sizing system, *J. Inst. Energy* **9**, 119–123 (1981).
14. G. P. Bertolini, L. M. Oberdier and Y. H. Lee, Image processing system to average droplet distributions in sprays, *Optical Engng* **24**(3), 464–469 (1985).
15. E. L. Hanzevack, C. B. Bowers, Jr. and C. H. Ju, Study of two phase flow by laser image processing, *A.I.Ch.E. Jl* **33**(12), 2003–2007 (1987).
16. K. D. Ahlers and D. R. Alexander, Microcomputer based digital image processing system developed to count and size laser—generated small particle images, *Optical Engng* **24**(6), 1060–1065 (1985).
17. I. G. Kim and S. Y. Lee, A simple technique for sizing and counting spray drops using digital image processing, *Exp. Thermal Fluid Sci.* **3**, 214–221 (1990).
18. S. Kannan, Experimental study of two-liquid swirling flows in a hydrocyclone using flow visualization and digital image processing. M.S. Thesis, Department of Mechanical Engineering, Clemson University, Clemson, SC (1991).
19. K. R. Castleman, *Digital Image Processing*. Prentice-Hall, Englewood Cliffs, NJ (1979).

APPENDIX: FIRST ORDER MODELING OF THE SYSTEM

The oil concentration in any plane of the cylinder increased monotonically with time and subsequently levelled off, indicating that at the flow rates observed the cyclone may be behaving as a mixer or a well stirred reactor. To test this conclusion, the cyclone was modeled as a first order system with the following analysis.

Consider the cylinder to be a control volume into which water and oil enter with flow rates $q_{w,in}$ and $q_{oil,in}$, respectively. The mass conservation equation for oil can be written as

$$\left(\frac{dM_{oil}}{dt}\right)_{C.V.} = \dot{m}_{oil,in} - \dot{m}_{oil,out} \tag{A.1}$$

or in terms of the volumetric flow rate as

$$\left(\frac{dV_{oil}}{dt}\right)_{C.V.} = q_{oil,in} - q_{oil,out}. \tag{A.2}$$

The volume flow rates can now be expressed as

$$q_{oil,in} = q_{in} \times C_{oil,in}$$
$$q_{oil,out} = q_{out} \times C_{oil,out}$$
$$V_{oil,C.V.} = V_{C.V.} \times C_{oil,out}$$

where

$$q_{in} = q_{out} = \text{flow rate of the mixture} = q_{mixture}.$$

Equation (A.2) now becomes,

$$V_{C.V.}\frac{dC_{oil,out}}{dt} = q_{in}C_{oil,in} - q_{out}C_{oil,out} \tag{A.3}$$

which can be rearranged as

$$\frac{dC}{dt} = \frac{q_{mixture}}{V_{C.V.}}[1 - C] \tag{A.4}$$

where

$$C = \frac{C_{oil,out}}{C_{oil,in}}.$$

Also, if

$$\tau = \frac{V_{C.V.}}{q_{mixture}}$$

the differential equation (A.4) becomes

$$\tau\frac{dC}{dt} = 1 - C. \tag{A.5}$$

Equation (A.5) is the first order governing equation for oil concentration in the cylinder. With the initial condition $C(t = 0) = 0$, the above equation can be easily solved to give

$$C(t) = 1 - e^{-(t/\tau)}. \tag{A.6}$$

Equation (A.6) represents the variation of oil concentration with time. t is the time constant of the system, and is defined as the time for the concentration to attain 63.6% of its value at infinite time. For 5 and 4 GPM, the time constants were calculated to be 41.7 and 52.6 s, respectively.